Chaos and quantum fluctuations in the Hénon-Heiles and four-leg potentials

Lee Carlson and W. C. Schieve
Center for Studies in Statistical Mechanics, University of Texas at Austin, Austin, Texas 78712
(Received 1 May 1989)

Using the idea of the Gaussian effective potential due to Stevenson [Phys. Rev. D **30**, 1712 (1984)], the effect of quantum fluctuations on chaotic behavior is studied in the Hénon-Heiles and four-leg potentials.

I. INTRODUCTION

In this work the effects of quantum fluctuations in the Hénon-Heiles[1] potential and what we call the four-leg potential are studied using the Gaussian effective potential.[2] In the papers of Churchhill, Pecelli, and Rod[3] (CPR), these two potentials were shown to exhibit chaotic behavior for certain restricted energy ranges. They show that due to their symmetry properties these potentials have periodic orbits and that, as the result of geometrical conditions, these periodic orbits are also hyperbolic. Also, by numerically proving the existence of a so-called "crossing" orbit in these potentials, they showed that the unstable manifold of one periodic orbit intersects the stable manifold of another periodic orbit, with the intersection being topologically transverse, all this taking place in a bounded region around the origin. Thus there is a horseshoe[4] in the dynamics based on these potentials.

The interested reader can find an outline of the CPR conditions in Appendix A. We will not elaborate on their results as they are very lengthy and quite abstract. For more details we refer the reader to their original papers.[3] In Sec. II the Gaussian effective potential (GEP) will be reviewed and calculated for the Hénon-Heiles potential and the four-leg potential. We will then plot the GEP for various values of Planck's constant and for some energy ranges where crossing orbits are known to exist. It is found that the effect of quantum fluctuations is to "close off" the "legs" of these potentials and result in a potential that is merely a circle around the origin. In Sec. III we will examine one of the CPR conditions and study the effect of quantum fluctuations on this condition. Lastly, in Sec. IV we draw some conclusions.

II. THE GAUSSIAN EFFECTIVE POTENTIAL

To examine the effects of quantum fluctuations on the chaotic behavior in the above potentials we will use the idea of the Gaussian effective potential due to Stevenson.[2] In general, the effective potential of a system gives us a picture of how the quantum fluctuations modify the classical potential. In particular, for a particle in a potential well(s), the Heisenberg uncertainty principle implies that if the particle's wave function is concentrated in a small region ΔX, then the momentum uncertainty is very large: $\Delta P \geq h/\Delta X$. There is then a large contribution to the energy arising from the kinetic energy $\langle P^2/2 \rangle$. This means that the ground-state energy is a function of the depth *and* the width of the potential wells. In a symmetric double well, for example, the quantum fluctuations lower the barrier since the particle can spread itself out and lower its energy. But because of the zero-point energy, the energy is higher in the wells. The idea of Stevenson is to approximate the effective potential of a system by using Gaussian wave functions. We will construct this quantity for systems with two spatial degrees of freedom. For such a system with Hamiltonian $H(p_1,p_2,x,y)$, we first compute the expectation value of the energy

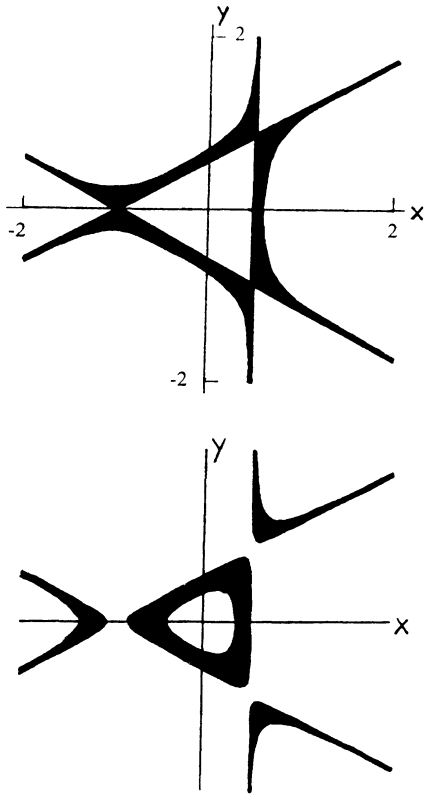

FIG. 1. Here $\frac{1}{6} < V_G < \frac{1}{4}$. The top diagram is for $h=0$; the bottom for $h=0.1$.

$$\langle F|H|F\rangle \ , \tag{2.1}$$

where the normalized wave functions F are two-dimensional Gaussians of the form $\exp(-x_j\Omega_{ij}x_j/2)$ and where Ω_{ij} is a symmetric matrix that in general depends on the position variables. The *Gaussian effective potential* is defined as

$$V_G(x,y)=\min_\Omega\langle F|H|F\rangle \ . \tag{2.2}$$

One will note that this is an ansatz which involves three parameters: two principal frequencies Ω, w, and an angle β which specifies the orientation of the principal axes of the wave function with respect to the x,y axes. The two frequencies and the angle are adjusted to minimize $\langle F|H|F\rangle$ at each x,y. Using the number representation

$$\begin{bmatrix}x_1\\x_2\end{bmatrix}=\begin{bmatrix}x\\y\end{bmatrix}\begin{bmatrix}\cos\beta & -\sin\beta\\ \sin\beta & \cos\beta\end{bmatrix}\begin{bmatrix}(2\Omega)^{-1/2}(a_1+a_1^\dagger)\\ (2w)^{-1/2}(a_2+a_2^\dagger)\end{bmatrix},$$

$$\begin{bmatrix}p_1\\p_2\end{bmatrix}=\begin{bmatrix}\cos\beta & -\sin\beta\\ \sin\beta & \cos\beta\end{bmatrix}\begin{bmatrix}-(i/2)(2\Omega)^{1/2}(a_1-a_1^\dagger)\\ -(i/2)(2w)^{1/2}(a_2-a_2^\dagger)\end{bmatrix},$$

where $[a_1,a_1^\dagger]=1$ and $[a_2,a_2^\dagger]=1$, the expectation value of H is evaluated in the state $|0\rangle_\Omega$ defined by

$$a_1|0\rangle_\Omega=0 \text{ and } a_2|0\rangle_\Omega=0 \ .$$

The Hénon-Heiles Hamiltonian is given by

$$H=(p_1^2+p_2^2)/2+(x_1^2+x_2^2)/2-x_1x_2^2+x_1^3/3 \ . \tag{2.3}$$

The Gaussian effective potential for the Hénon-Heiles system is given by

$$\begin{aligned}V_G=&(x^2+y^2)/2-xy^2+x^3/3\\ &+(h/2)\Omega^{-1}+w^{-1})(x\cos\beta-y\sin\beta)\\ &+(h/4)(\Omega+w) \ ,\end{aligned} \tag{2.4}$$

where

$$\Omega=(2x\cos\beta-2y\sin\beta+1)^{1/2} \ ,$$

$$w=(1-2x\cos\beta+2y\sin\beta)^{1/2} \ ,$$

and

$$\beta=(\tfrac{1}{2})\arctan(-y/x) \ .$$

For the four-leg potential with

$$H=(p_1^2+p_2^2)/2+(x^2+y^2)/2-x^2y^2/2 \ ,$$

the Gaussian effective potential is calculated to be

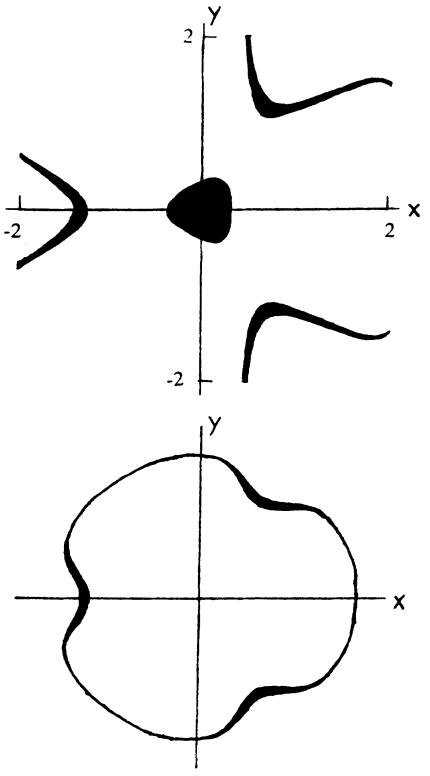

FIG. 2. Here $\frac{1}{6}<V_G<\frac{1}{4}$. The top diagram is for $h=0.2$; the bottom for $h=0.3$.

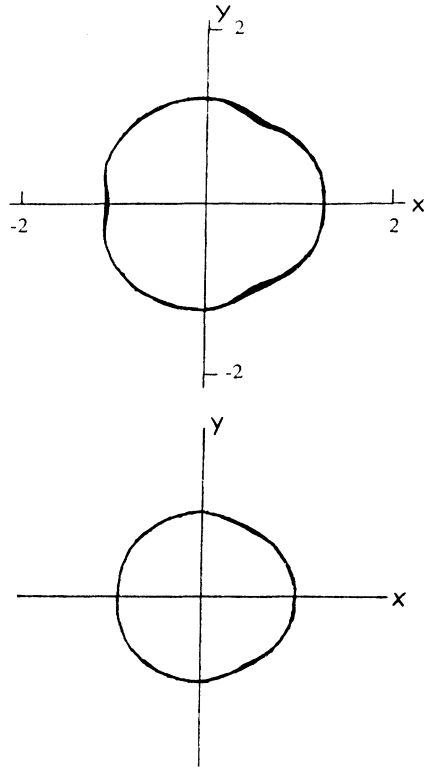

FIG. 3. Here $\frac{1}{6}<V_G<\frac{1}{4}$. The top diagram is for $h=0.4$; the bottom for $h=0.5$.

$$V_G=(x^2+y^2)/2-x^2y^2/2+(2\Omega^2)^{-1}+(2w^2)^{-1}$$
$$-3(4\Omega)^{-1}-3(4w)^{-1}-(2\Omega w)^{-1}$$
$$+2\Omega^{-1}(x\cos\beta+y\sin\beta)^2$$
$$+2w^{-1}(-x\sin\beta+y\cos\beta)^2+(\Omega+w)/4\ ,$$

where $\beta=\arctan(y/x)$. Ω and w are found from the equations

$$\Omega^3+\Omega[3+2w^{-1}-8(x\cos\beta+y\sin\beta)^2]-4=0\ , \quad (2.5a)$$

$$w^3+w[3+2\Omega^{-1}-8(-x\sin\beta+y\cos\beta)^2]-4=0\ . \quad (2.5b)$$

These equations must be solved simultaneously to give Ω and w. Unfortunately, when Ω is expressed in terms of w from Eq. (2.10b) and then inserted into Eq. (2.10b), the resulting equation for Ω is of fifth degree and therefore must be solved numerically for each value of x and y.

In Figs. 1–8 the level curves of V_G are plotted for the Hénon-Heiles potential at various energies where crossing orbits are known to exist and for various values of Planck's constant. In the figures Planck's constant is scaled to 1. Also, in Fig. 9, V_G is plotted for the four-leg potential (for Planck's constant equal to 1) at the energy gap range $1.5<V_G<3$ where CPR have shown the existence of crossing orbits. It is seen that the $2\pi/3$ symmetry is preserved by the quantum fluctuations in the Hénon-Heiles potential and the $\pi/4$ symmetry is preserved by the quantum fluctuations in the four-leg potential. For the Hénon-Heiles system in the energy range $\frac{1}{6}<V_G<\frac{1}{4}$, one observes that the "legs" of the Hénon-Heiles potential "close off" when Planck's constant is equal to 0.3. One can see this explicitly by calculating the transverse width w of the Gaussian wave function from Eq. (2.9). For example, at $\mathbf{X}=(-1,0)$ and when $V=\frac{1}{4}$, the width of the "corrider" is $\frac{2}{3}\sqrt{2}$, while the transverse width of the wave function is equal to $\sqrt{3}$. For the energy range $\frac{2}{3}<V_G<\frac{5}{6}$ the legs close off when Planck's constant is equal to 0.7. The closing off of the legs is a consequence of the Heisenberg uncertainty principle: A wave packet tends to avoid regions where grad$V$ is large, which here are the regions along the gradient lines of the potentials.

Also, just as in the Hénon-Heiles potential, the quantum fluctuations close off the legs in the four-leg potential and result in an effective potential that is simply a circle around the origin.

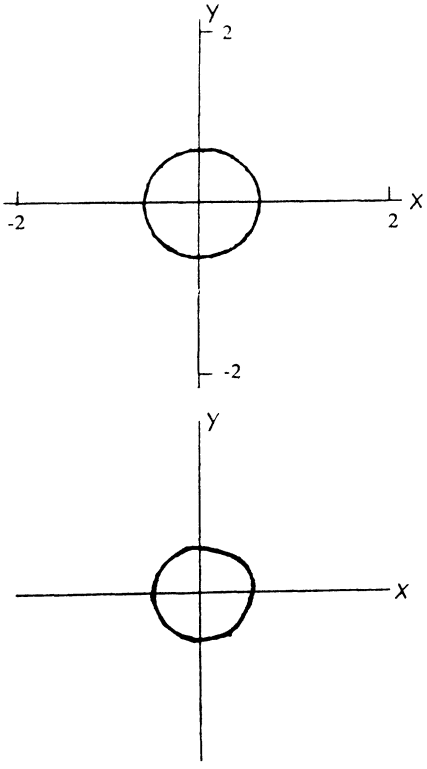

FIG. 4. Here $\frac{1}{6}<V_G<\frac{1}{4}$. The top diagram is for $h=0.8$; the bottom for $h=0.9$.

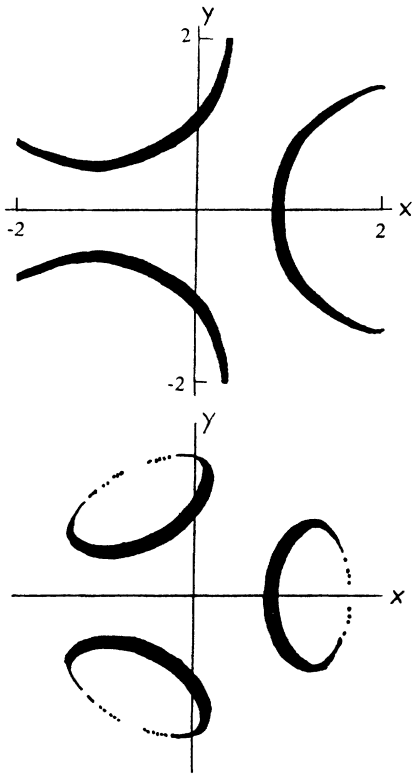

FIG. 5. Here $\frac{2}{3}<V_G<\frac{5}{6}$. The top diagram is for $h=0.2$; the bottom for $h=0.3$.

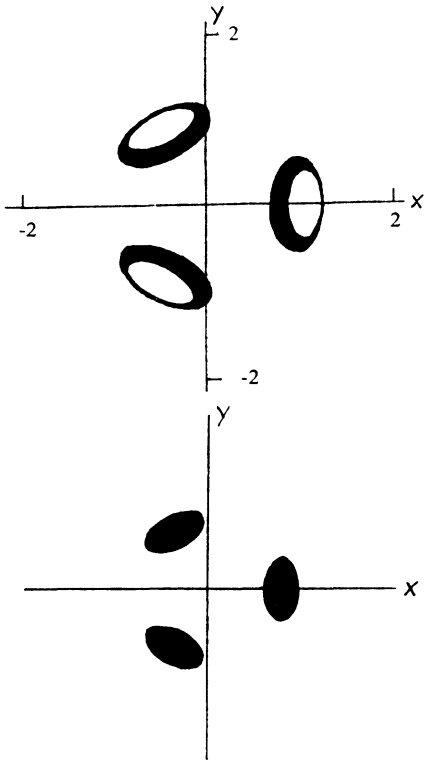

FIG. 6. Here $\frac{2}{3} < V_G < \frac{5}{6}$. The top diagram is for $h = 0.4$; the bottom for $h = 0.5$.

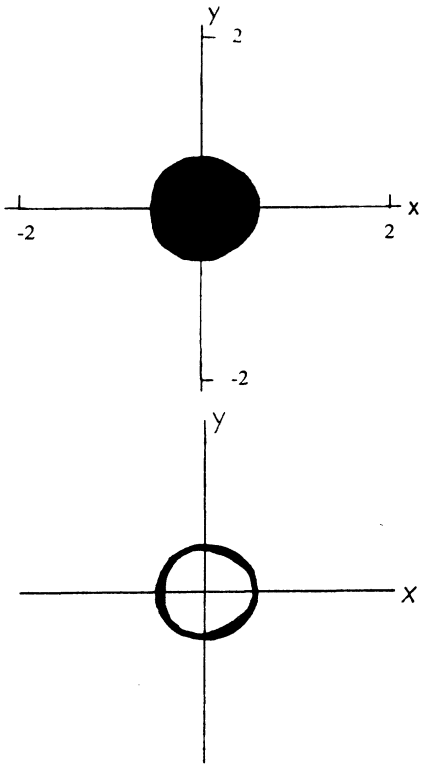

FIG. 7. Here $\frac{2}{3} < V_G < \frac{5}{6}$. The top diagram is for $h = 0.8$; the bottom for $h = 0.9$.

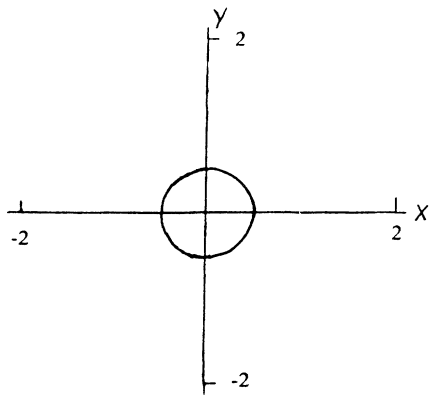

FIG. 8. Here $\frac{2}{3} < V_G < \frac{5}{6}$; $h = 1$.

III. QUANTUM FLUCTUATIONS AND THE HYPERBOLICITY CONDITIONS

It is also instructive to examine what happens to the conditions for hyperbolicity of the periodic orbits when quantum fluctuations are present. From Appendix A one of the conditions (condition 3) for hyperbolicity of the periodic orbit is that $\langle T, V \rangle$ be less than 0 above the critical energy. To examine the effect of quantum fluctuations on this quantity define the quantity $\langle T_G, V_G \rangle$ where V_G is the effective potential and $T_G = T + T'$, where T' is the vector field defined by

$$T' = JV'_{XX}JV'_X$$

and where V' is the quantum correction to the classical potential ($V_G = V + V'$). Written out in detail one has that

$$\begin{aligned}\langle T_G, V_G \rangle &= \langle T + T', V + V' \rangle \\ &= \langle T + T', V \rangle + \langle T + T', V' \rangle \\ &= \langle T, V \rangle + \langle T', V \rangle + \langle T, V' \rangle + \langle T', V' \rangle\end{aligned}$$

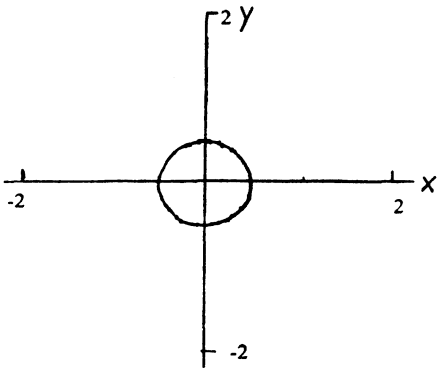

FIG. 9. Here $1.5 < V_G < \frac{5}{6}$ and $h = 1$.

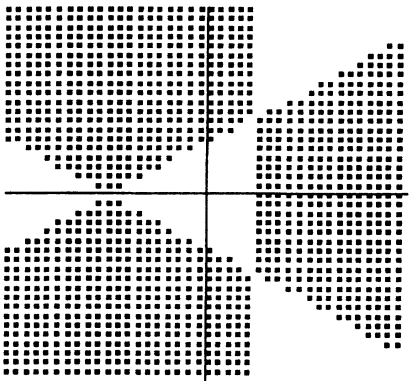

FIG. 10. Here $h=0$ and the shaded region is where $\langle T_G, V_G \rangle < 0$.

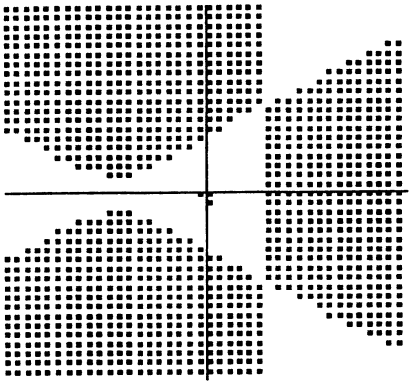

FIG. 11. Here $h=0.1$ and the shaded region is where $\langle T_G, V_G \rangle < 0$.

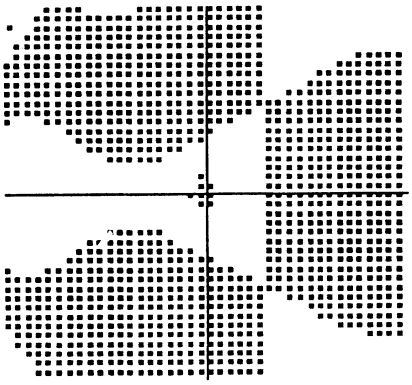

FIG. 12. Here $h=0.2$ and the shaded region is where $\langle T_G, V_G \rangle < 0$.

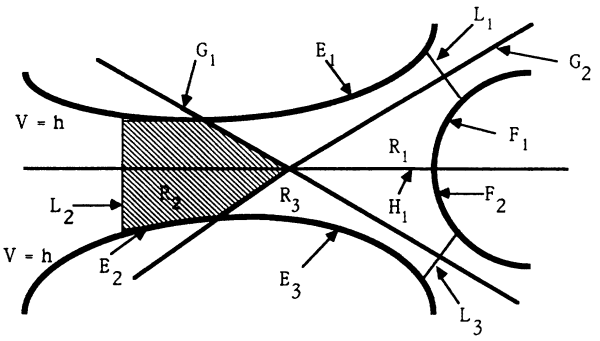

FIG. 13. Diagram illustrating the regions R_i.

The calculations needed for obtaining the above quantities are given in Appendix B. If the quantity $\langle T_G, V_G \rangle$ is less than zero in regions where $\langle T, V \rangle$ is not, then we have a qualitative test of the effects of quantum fluctuations on the hyperbolicity of the periodic orbits. In Figs. 10–13 the regions where $\langle T_G, V_G \rangle$ is less than zero is plotted for Planck's constant equal to 0, 0.1, and 0.2. It is seen that when Planck's constant is equal to 0.1, there is a region around the origin where $\langle T_G, V_G \rangle$ is less than zero. This region around the origin is even larger when Planck's constant is equal to 0.2. These figures imply that due to the quantum fluctuations the level curves of V are becoming concave up in this region where they were strictly concave down without the quantum fluctuations. Physically this is because (effectively) a wave packet does not spill over the corridor in the directions of the gradient lines, but stays near the origin.

We should remark here that we have not plotted the quantity $\langle T_G, V_G \rangle$ for values of Planck's constant above 0.2. We have not done this since it is our contention that although the Gaussian effective potential is not a semiclassical quantity, the T-vector field is not really a meaningful quantity except for values of Planck's constant close to zero, since it was defined for a specific geometry.

IV. CONCLUSIONS

In both of these cases above it is seen that as Planck's constant gets closer to 1, the effective potential is a circle around the origin which is, of course, completely integrable. It is in this sense that the quantum fluctuations destroy the chaotic behavior in the Hénon-Heiles potential and in the four-leg potential. To be more specific, solving Newton's equations of motion using the effective potential

$$\frac{d^2x}{dt^2} = -\text{grad}V_G$$

will give the motion of the center x of a Gaussian wave packet in the Hénon-Heiles potential. When V_G is a circle (as it is above) the dynamics of the wave packet is equivalent to the dynamics of a particle in a classical two-dimensional harmonic oscillator, which is integrable.

In using the Gaussian effective potential one would

naturally wonder just how good an approximation it is. Munoz-Tapia *et al.*[5] have defined an uncertainty for the Gaussian effective potential in one dimension. They demonstrated that the uncertainty of the GEP for the ordinary harmonic oscillator vanishes identically, just as one might expect. Using a generalization of their definition to two-dimensional potentials the uncertainty of the GEP in the Hénon-Heiles potential was shown[6] to vanish at the origin and grew larger as one moved away from the origin. But it is only in the region around the origin that the CPR theory is applicable, thus giving more credence to the use of the GEP in the study of quantum effects in the Hénon-Heiles potential. In Ref. 6 GEP was also used to study the evolution of a scalar field in a time-dependent potential assuming a Robertson-Walker background spacetime.

Although we have not proved absolutely that chaos is suppressed by quantum fluctuations in these potentials (since the GEP is only an approximation to the actual quantum mechanics), the approach used here shows some promise to study this very difficult problem. One should note that much use has been made of the particular geometry of the potentials to show the existence of chaos and to study the effects of quantum fluctuations on this chaos. In this spirit the authors in Ref. 7 studied the effects of quantum fluctuations on the chaos in the forced Duffing oscillator using a semiclassical generalization of the Melnikov function.[8] Also in Ref. 9 chaos was shown to exist in the squeezed double-well potential[10] using generalized Melnikov techniques due to Holmes and Marsden.[11] The reflection symmetry in the squeezed double-well potential was used to study the effect of quantum fluctuations around the instanton path on the chaotic behavior.

The CPR theory and the Melnikov techniques are both tools that allow one to show the existence of chaos *analytically*. These two developments, however, are only applicable to a very restricted class of potentials, most physical systems of interest do not have the geometrical properties required to use these techniques. Therefore it is of great interest to find other analytic techniques to show the existence of chaos.

APPENDIX A: THE CHURCHILL-PECELLI-ROD THEORY

Let M be an energy surface for a dynamical system with a real analytic Hamiltonian H which is defined on a four-dimensional real analytic symplectic manifold. Also, let $\mathbf{X}$ be a point in the plane $\mathbb{R}^2$ and let $V(\mathbf{X})$ be a potential that is differentiable to third order. Let $H=h$ be the three-manifold $\{\mathbf{X},\mathbf{Y}$ in $\mathbb{R}^2 | H(\mathbf{X},\mathbf{Y})=\frac{1}{2}|\mathbf{Y}|^2+V(\mathbf{X})=h\}$ of solutions of energy h of Hamiltonian's equations

$$\frac{d\mathbf{X}}{dt}=\mathbf{Y}\ ,\quad d\mathbf{Y}/dt=-V_{\mathbf{X}}\ .$$

Let $P(\mathbf{X},\mathbf{Y})=\mathbf{X}$ be the projection of $H=h$ into the $\mathbf{X}$ plane. $H=h$ projects to $\{\mathbf{X}|V(\mathbf{X})\le h\}$. This region will be referred to as $V(\mathbf{X})\le h$. A line L in the $\mathbf{X}$ plane is a gradient line of V if for each point p in L then the gradient $V_{\mathbf{X}}(p)$ is parallel to L.

The examples we will study will satisfy the following geometric hypothesis: There is a critical energy h_0 such that for $h>h_0$ the region $V(X)<h$ has a bounded subregion containing the origin which is the union of closed two-dimensional regions R_i, $i=1,\ldots,N$ where $N\ge 3$ with the following properties.

(1) The boundary of R_i consists of two segments E_i and F_i, one on each of the distinct branches of the level curve $V=h$. Also, there is a line L_i connecting an endpoint of E_i with one of F_i and two gradient line segments G_i and H_i of the potential V connecting the other endpoints of E_i and F_i to the origin.

(2) For $i\neq j$, the interior of R_i does not intersect the interior of R_j and the intersection of the boundary of R_i with the boundary of R_j consists either solely of the origin, or of one gradient line segment from $V=h$ to the origin.

(3) All gradient lines of V pass through the origin. Each region R_i is separated into two components by one and only one such gradient line, and this line intersects L_i (see Fig. 13).

Now suppose V is a real-valued potential that is third-order differentiable and is defined on some open region of the plane. It will be assumed that there is a periodic solution Π of $d^2X/dt^2=-V_{\mathbf{X}}$ with energy $h=|d\mathbf{X}/dt|^2/2+V(\mathbf{X})$ that connects points p and p' on two distinct branches of the level curve $V(\mathbf{X})=h$. These branches will be separated by a gradient line of the potential. This gradient line will be called A. The branch containing p is called the upper branch and is assumed to be strictly concave up with respect to A. The branch containing p' is called the lower branch and is assumed to be strictly concave down with respect to A (see Fig. 14).

The gradient $V_{\mathbf{X}}$ will be assumed to be nonzero off A and to have values above (below) A in the upper (lower) half-plane determined by A. All this implies that there is an h_0 such that the level curves $V(\mathbf{X})=L$ for $h_0<L<h$ are smooth and have the right convexity properties. Now parametrize the upper branch of $V=h$ by a third-order differentiable function $f(s)$ of arclength s with $s=0$ at p and increasing to the right of p. By assumption on the direction of the gradient, orbits $\mathbf{x}(t,s)$ of energy h that begin at $\mathbf{x}(0,s)=f(s)$ on $V=h$ and with velocity $\mathbf{y}(0,s)=0$ at time $t=0$ fall toward A and intersect the

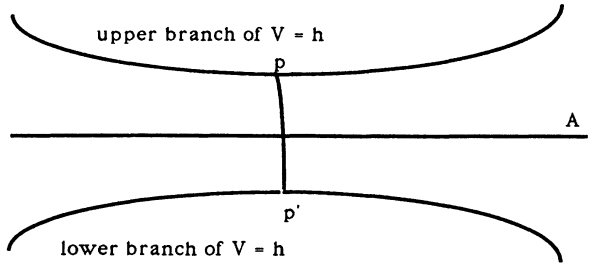

FIG. 14. The branches of the potential and the periodic orbit π.

level curves $V=L$ transversely for $h_0 \le L \le h$. Transversality implies that the time $t(L,s)$ required for $\mathbf{x}(t,s)$ to fall from $f(s)$ on $V=h$ to $V=L$ is a differentiable function of s. For $s \to 0$ define $\mathbf{X}(T,s)$ as the orbit rising from the lower branch of $V=h$ and intersecting the upper branch of $V=L$ transversely at $x(t(L,s),s)$ at positive time $T(L,s)$. Let $d\mathbf{x}/dt=\mathbf{y}$, $d\mathbf{X}/dt=\mathbf{Y}$, and $\mathbf{z}^*=\mathbf{z}/|\mathbf{z}|$ for any $\mathbf{z} \neq 0$. Also define a rotation matrix J by

$$J=\begin{bmatrix} 0 & 1 \\ -1 & 0 \end{bmatrix}$$

(J rotates vectors by an angle $-\pi/2$) and define the normalization operation, denoted by an asterisk, by $V_x^*(L)=[V_x(x(t(L,0),0))]^*$. Now remembering that the curvature k of a curve $\mathbf{x}(t)$ in the plane is given by

$$k(\mathbf{x}(t))=-\left|\frac{d\mathbf{x}}{dt}\right|^{-3}\left\langle \frac{d^2\mathbf{x}}{dt^2}, J\frac{d\mathbf{x}}{dt}\right\rangle .$$

The strategy of CPR is to use the velocity vectors to investigate the curvature properties of the orbits by first defining constants $a(L)$ that will normalize $a(L,0)=0=b(L,0)$:

$$a(L,s)=a(L)-\arccos\langle V_{\mathbf{x}}^*(L), J\mathbf{y}^*(t(L,s),s)\rangle ,$$

$$b(L,s)=a(L)-\arccos\langle V_{\mathbf{x}}^*(L), J\mathbf{Y}^*(T(L,s),s)\rangle .$$

CPR then uses these ideas to show the Poincaré mapping associated with the periodic orbit π is hyperbolic. In doing this they assume the following hypothesis.

Transversability hypothesis. There is an $L, h_0 < L < h$ for which $(\partial a/\partial s)(L,0) > 0$.

Foliation hypothesis. For the same L of the transversability hypothesis and $s_1 < s_2$ close to zero, the orbits $\mathbf{x}(t,s_1)$ and $\mathbf{x}(t,s_2)$ do not intersect in falling from $V=h$ to $V=L$ and $a(L,s_1) < a(L,s_2)$. Furthermore, the orbits $\mathbf{X}(T,s_1)$ and $\mathbf{X}(T,s_2)$ do not intersect on rising from the lower branch of $V=h$ to the upper branch of $V=L$, and $b(L,s_1) > b(L,s_2)$ (see Fig. 15).

In Ref. 4 it is proven that given a potential V with the above properties, the transversality and foliation hypotheses imply that the periodic orbit $(\pi, d\pi/dt)$ is hyperbolic on the manifold of solutions of $d\mathbf{x}/dt=\mathbf{y}$, $d\mathbf{y}/dt=-V_{\mathbf{x}}$ with energy h.

For each problem one considers the above hypotheses must be verified. We refer the interested reader to Ref. 4

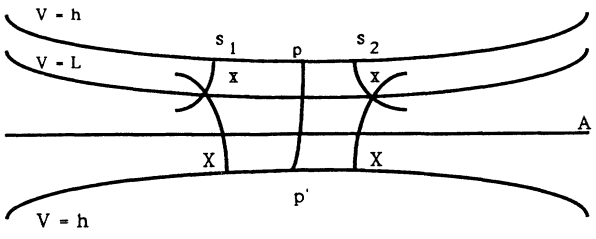

FIG. 15. Diagram illustrating the foliation hypothesis.

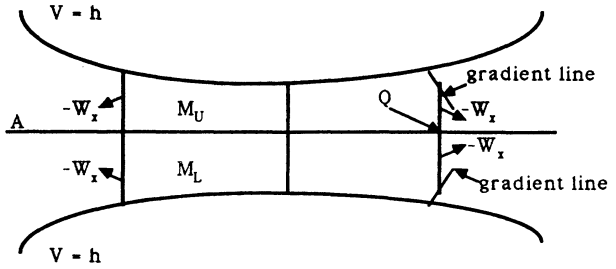

FIG. 16. Illustration of the regions M_U and M_L.

for the verification of the transversality hypothesis. Checking the foliation hypothesis depends on five conditions on the potential V. We will elaborate on these conditions because we will examine the effect of quantum fluctuations on one of the conditions later. First construct a set M' containing the periodic orbit π by intersecting $\{\mathbf{x} | V(\mathbf{x}) \le h\}$ with a vertical strip so that the right boundary of this strip intersects the gradient line A at the only critical point Q of V in M'. Now remove from M' any gradient lines of the potential other than A and define M to be the closure of that component of the remaining set that contains π. The line A divides M into two closed regions, denoted by M_U and M_L (see Fig. 16). The following five conditions that imply the foliation hypothesis.

Condition 1. The gradient field $V_{\mathbf{x}}$ restricted to the portion of A in $M-\{Q\}$ points towards Q and in $M_U - A$ points into the upper half plane determined by A.

Condition 2. The equation $\operatorname{div}(JV_{\mathbf{x}}/|JV_{\mathbf{x}}|) > 0$ is in the interior of M_U.

Condition 3. The level curve $V=h_0=V(Q)$ is a straight line issuing from Q and intersecting M_U as in Fig. 16. For energies $L > h_0$ the level curves $V=K$ in M_U are strictly concave up with respect to A, while for $L < h_0$ they are strictly concave down (see Fig. 17).

Condition 4. All orbits $\mathbf{x}(t,s)$ of $d^2\mathbf{x}/dt^2=-V_{\mathbf{x}}$ with energy $h > h_0$ that originate at $\mathbf{x}(0,s)=f(s)$ on $V=h$ cross the integral curves of $T=-JV_{\mathbf{xx}}JV_{\mathbf{x}}$ transversely

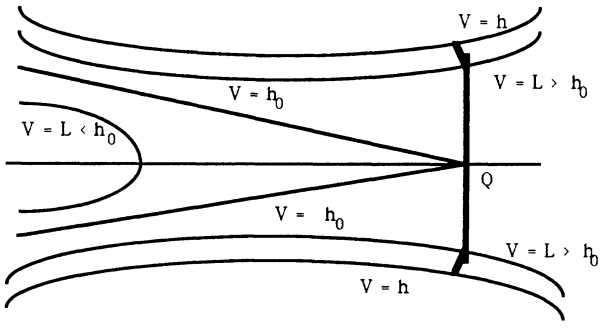

FIG. 17. Diagram illustrating the concavity of the level curves.

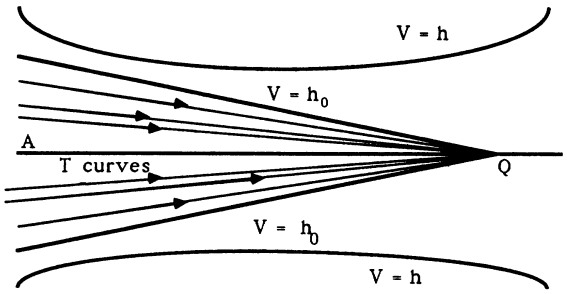

FIG. 18. Diagram illustrating the integral curves of T.

in the subregion of $M_U-\{Q\}$ between and including the lines A and $V=h_0$ in falling from $V=h$ to A (see Fig. 18).

Condition 5. Consider any T curve in the subregion of $M_U-\{Q\}$ between and including the lines $V=h_0$ and A. Let $\mathbf{u}$ be any vector obtained as the unit tangent vector of an orbit of energy h rising to $V=h$ as it crosses this T curve. Then $\langle T,J\mathbf{u}\rangle<0$ and for $d=\det(V_{XX})$ one must have

$$\{[3d(h-V)+T(V)]\langle T,J\mathbf{u}\rangle - (h-V)\langle D_T T,J\mathbf{u}\rangle\}(\mathbf{X})<0$$

for all $\mathbf{X}$ along the T curve between the point of intersection and Q.

In Ref. 4 CPR show that these five conditions imply the foliation hypothesis.

To show the existence of chaotic behavior in the dynamical systems with these Hamiltonians, it also must be proven that the dynamical equations of motion possess what is called by CPR a *crossing orbit.* In Fig. 19 an illustration of a crossing orbit is given. CPR show that if such an orbit exists then the unstable manifold of one periodic orbit intersects the stable manifold of another topologically transverse. This gives an analog of the horseshoe phenomena of Smale.

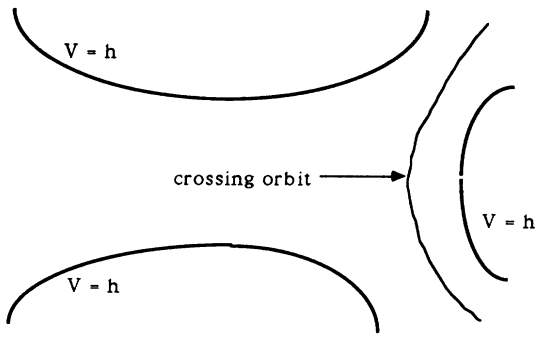

FIG. 19. Illustration of a crossing orbit.

APPENDIX B: CALCULATION OF T_G FOR THE HÉNON-HEILES POTENTIAL

For

$$V'=h(\tfrac{1}{2}\Omega+\tfrac{1}{2}w)(x\cos\beta-y\cos\beta)+h(\Omega+w)/4$$

one has

$$T'=\begin{bmatrix}0&-1\\1&0\end{bmatrix}\begin{bmatrix}V'_{xx}&V'_{yx}\\V'_{xy}&V'_{xy}\end{bmatrix}\begin{bmatrix}0&1\\-1&0\end{bmatrix}\begin{bmatrix}V'_x\\V'_y\end{bmatrix}=\begin{bmatrix}V'_{yy}V'_x-V'_{xy}V'_y\\V'_{xx}V'_y-V'_{yx}V'_x\end{bmatrix}.$$

The terms in this expression are given by

$$V'_x=(E_xD+ED_x)/2+h(\Omega_x+w_x)/4\ ,$$
$$V'_y=(E_yD+ED_y)/2+h(\Omega_y+w_y)/4\ ,$$
$$V'_{yx}=(DE_{yx}+E_xD_y+E_yD_x+ED_{yx})/2+h(\Omega_{yx}+w_{yx})/4\ ,$$
$$V'_{xy}=(E_{xy}D+E_yD_y+E_xD_y+ED_{xy})/2+h(\Omega_{xy}+w_{xy})/4\ ,$$
$$V'_{xx}=(E_{xx}D+E_xD_x+E_xD_x+ED_{xx})/2+h(\Omega_{xx}+w_{xx})/4\ ,$$
$$V'_{yy}=(E_{yy}D+E_yD_y+E_yD_y+ED_{yy})/2+h(\Omega_{yy}+w_{yy})/4\ .$$

Here

$$\beta=\arctan(-y/x)2\ ,$$
$$D=x\cos\beta-y\cos\beta\ ,$$

and

$$D_x=\cos\beta-(xy\sin\beta-y^2\cos\beta)/2L\ ,$$
$$D_y=(x^2\sin\beta+yx\cos\beta)/2L-\sin\beta\ ,$$
$$D_{xx}=(\cos\beta)_x-\{2L[y\sin\beta+xy(\sin\beta)_x]\}-4x^2y\sin\beta/4L^2-y^2[L(\cos\beta)_x+2y\cos\beta]/2L^2\ ,$$
$$D_{yx}=(\cos\beta)_y-5x\{L[\sin\beta+y(\sin\beta)_y]-2y^2\sin\beta\}/L^2-\{L[2y\cos\beta+y^2(\cos\beta)_y]+y^2(\cos\beta)_y\}-2y^3\cos\beta/2L^2\ ,$$
$$D_{xy}=\{L[2x\sin\beta+x^2(\sin\beta)_x]-2x^3\sin\beta\}/2L^2-(\sin\beta)_x+y\{L[\cos\beta+(\cos\beta)_x]-2x^2\cos\beta\}/2L^2\ ,$$
$$D_{yy}=x^2[L(\sin\beta)_y-2y\sin\beta]/2L^2-(\sin\beta)_y+x\{L[\cos\beta+y(\cos\beta)_y]-2y^2\cos\beta\}/2L^2\ ,$$
$$E=h(1/\Omega+1/w)\ ,$$
$$E_x=h(-\Omega_x/\Omega^2-w_x/w^2)\ ,$$

$$E_y = h(-\Omega_y/\Omega^2 - w_y/w^2) ,$$
$$E_{xx} = h(2\Omega_x^2/\Omega^3 - \Omega_{xx}/\Omega^2 + 2w_x^2/w^3 - w_{xx}/w^2) ,$$
$$E_{yy} = h(2\Omega_y^2/\Omega^3 - \Omega_{yy}/\Omega^2 + 2w_y^2/w^3 - w_{yy}/w^2) ,$$
$$E_{yx} = h(2\Omega_x\Omega_y/\Omega^3 - \Omega_{yx}/\Omega^2 + 2w_x w_y/w^3 - w_{yx}/w^2) ,$$
$$E_{xy} = h(2\Omega_x\Omega_y/\Omega^3 - \Omega_{xy}/\Omega^2 + 2w_x w_y/w^3 - w_{xy}/w^2) ,$$
$$\Omega_x = D_x/\Omega, \quad \Omega_y = D_y/\Omega, \quad w_x = -D_x/w, \quad w_y = -D_y/w$$
$$\Omega_{xx} = -\Omega_x D_x/\Omega^2 + D_{xx}/\Omega ,$$
$$\Omega_{yx} = -\Omega_y D_x/\Omega^2 + D_{yx}/\Omega ,$$
$$\Omega_{xy} = -\Omega_x D_y/\Omega^2 + D_{xy}/\Omega ,$$
$$\Omega_{yy} = -\Omega_y D_y/\Omega^2 + D_{yy}/\Omega ,$$
$$w_{xx} = w_x D_x/w^2 - D_{xx}/w ,$$
$$w_{yx} = w_y D_x/w^2 - D_{yx}/w ,$$
$$w_{xy} = w_x D_y/w^2 - D_{xy}/w ,$$
$$w_{yy} = w_y D_y/w^2 - D_{yy}/w ,$$

where

$$L = x^2 + y^2 ,$$
$$(\cos\beta)_x = -y\sin\beta/2L, \quad (\sin\beta)_x = y\cos\beta/2L ,$$
$$(\cos\beta)_y = x\sin\beta/2L, \quad (\sin\beta)_y = -x\cos\beta/2L ,$$
$$\Omega_x = D_x/\Omega, \quad \Omega_y = D_y/\Omega ,$$
$$w_x = -D_x/w, \quad w_y = -D_y/w .$$

[1]M. Hénon and C. Heiles, Astron. J. **71**, 73 (1964).
[2]P. M. Stevenson, Phys. Rev. D **30**, 1712 (1984).
[3]R. C. Churchill, G. Pecelli, D. L. Rod, J. Diff. Eqs. **17**, 329 (1975); **24**, 329 (1977); R. C. Churchill and D. L. Rod, *ibid.* **21**, 39 (1976); **21**, 66 (1976); **37**, 23 (1980).
[4]S. Smale, Bull. Amer. Math. Soc. **13**, 747 (1967).
[5]R. Munoz-Tapia, J. Taron, and R. Tarrach, Int. J. Mod. Phys. **3**, 2143 (1988).
[6]Lee Carlson, Ph.D. dissertation, University of Texas at Austin, 1988.
[7]T. Petrosky and W. C. Schieve, Phys. Rev. A **31**, 3097 (1985).
[8]V. K. Melnikov, Trans. Moscow Math. Soc. **12**, 1 (1963).
[9]L. Carlson and W. C. Schieve, Phys. Rev. A **40**, 1127 (1989).
[10]A. Auerbach and S. Kivelson, Nucl. Phys. **B257**, 799 (1985).
[11]P. Holmes and J. Marsden, Commun. Math. Phys. **82**, 523 (1982).